Earth and Planetary Science Letters 578 (2022) 117283

Contents lists available at ScienceDirect

Earth and Planetary Science Letters

www.elsevier.com/locate/epsl

Molybdenum isotope systematics of lavas from the East Pacific Rise: Constraints on the source of enriched mid-ocean ridge basalt

Shuo Chen[a,b,*], Pu Sun[a,b,*], Yaoling Niu[b,c,d], Pengyuan Guo[a,b], Tim Elliott[e], Remco C. Hin[f]

[a] *Key Laboratory of Marine Geology and Environment, Institute of Oceanology, Chinese Academy of Sciences, Qingdao 266071, China*
[b] *Laboratory for Marine Geology, Pilot National Laboratory for Marine Science and Technology (Qingdao), Qingdao 266061, China*
[c] *Department of Earth Sciences, Durham University, Durham DH1 3LE, UK*
[d] *China University of Geosciences, Beijing 100083, China*
[e] *Bristol Isotope Group, School of Earth Sciences, University of Bristol, Bristol BS8 1RJ, UK*
[f] *Bayerisches Geoinstitut, Universität Bayreuth, Bayreuth 95447, Germany*

ARTICLE INFO

Article history:
Received 16 August 2021
Received in revised form 22 October 2021
Accepted 3 November 2021
Available online 22 November 2021
Editor: L. Coogan

Keywords:
molybdenum isotope
mid-ocean ridge basalt
East Pacific Rise
mantle heterogeneity

ABSTRACT

Mid-ocean ridge basalts (MORB) reveal large mantle compositional heterogeneity, whose origin remains debated. Here we present a systematic study of molybdenum isotopes on well-characterized MORB glass samples from the East Pacific Rise (EPR) and near-EPR seamounts. Our analyses show significant Mo isotope variations with $\delta^{98/95}$Mo (relative to NIST SRM3134) ranging from -0.23‰ to -0.06‰. We argue that these Mo isotope variations are not caused by processes of MORB melt generation and evolution but reflect mantle isotopic heterogeneity. Taking together with the literature data, we show that MORB Mo isotope compositions vary systematically with geochemical parameters indicating mantle enrichment. These observations are best explained by two-component mixing between an incompatible element depleted endmember (e.g., low La/Sm, Nb/La, Nb/Zr and Th/Yb, and high Sm/Nd and ^{143}Nd/^{144}Nd) with low $\delta^{98/95}$Mo (~-0.21‰) and an incompatible element enriched endmember (e.g., high La/Sm, Nb/La, Nb/Zr and Th/Yb, and low Sm/Nd and ^{143}Nd/^{144}Nd) with high $\delta^{98/95}$Mo (~-0.05‰). The association of heavier Mo isotope compositions with the geochemically more enriched MORB is inconsistent with recycled ocean crust with or without sediment being the enriched endmember. Instead, this is consistent with the enriched endmember being of magmatic origin, most likely lithologies of low-degree melt metasomatic origin dispersed in the more depleted peridotite matrix in the MORB mantle. Thus, with MORB Mo isotope systematics, we confirm that recycled oceanic mantle lithosphere metasomatized by low degree melt plays a key role in the formation of E-MORB source lithologies. Our study also highlights Mo isotopes as an effective tool for studying upper mantle processes.

1. Introduction

Studies of mid-ocean ridge basalts (MORB) and near-ridge seamounts have shown large sub-ridge mantle compositional heterogeneity on various scales (Allègre and Turcotte, 1986; Batiza and Niu, 1992; Donnelly et al., 2004; Niu et al., 2002; Waters et al., 2011; Zindler et al., 1984). The origin of these heterogeneities has been highly debated with interpretations including source region addition of recycled crustal materials, mantle wedge materials and low-degree melt metasomatism (Donnelly et al., 2004; Hofmann, 1997; Niu et al., 2002; Stracke, 2012). Radiogenic isotopes have been widely used to identify specific recycled components, but their interpretations are not unique (Elliott et al., 2006). Recently, a growing body of literature has shown that a combination of stable isotopes and radiogenic isotopes can be used to provide new perspectives on recycled materials (Andersen et al., 2015; Elliott et al., 2006; Nebel et al., 2019; Sun et al., 2020; Wang et al., 2018). In particular, stable Mo isotope systematics have great potential for studying mantle heterogeneities, especially those subduction-related processes (Chen et al., 2019a; Freymuth et al., 2015; König et al., 2016; Willbold and Elliott, 2017). For instance, high $\delta^{98/95}$Mo ($\delta^{98/95}\text{Mo} = [(^{98}\text{Mo}/^{95}\text{Mo}_{\text{sample}}/^{98}\text{Mo}/^{95}\text{Mo}_{\text{standard}}) - 1]$, where the subscript standard refers to the National Institute of Standards and Technology (NIST) reference material 3134) have been observed in mafic arc lavas with evidence for slab fluid inputs (Freymuth et al., 2015; König et al., 2016), while low $\delta^{98/95}$Mo has

---

* Corresponding authors at: Key Laboratory of Marine Geology and Environment, Institute of Oceanology, Chinese Academy of Sciences, Qingdao 266071, China.
E-mail addresses: shuochen@qdio.ac.cn (S. Chen), pu.sun@qdio.ac.cn (P. Sun).

https://doi.org/10.1016/j.epsl.2021.117283
0012-821X/

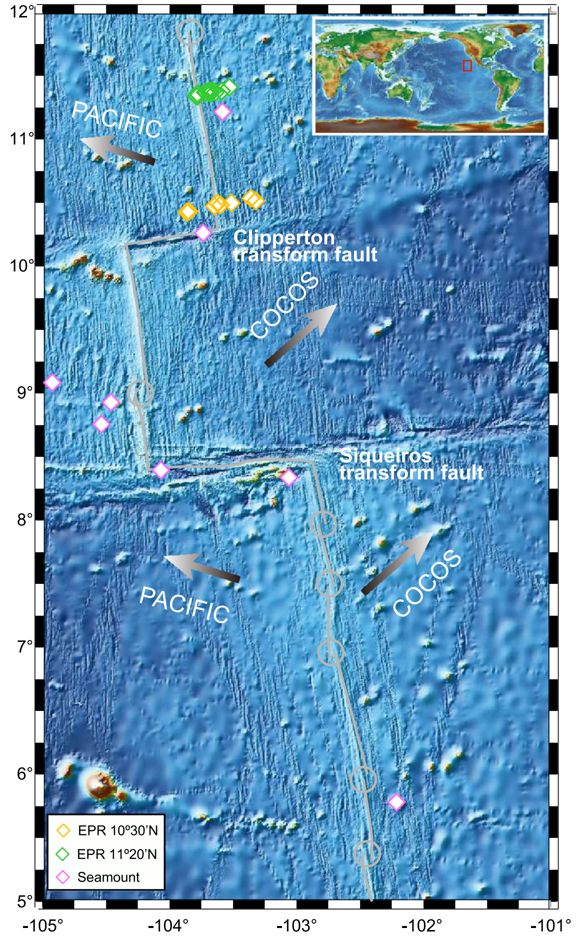

Fig. 1. Simplified map of the EPR between 5° and 12°N and samples investigated for Mo isotopes in this study. Base map is generated using GMT (the Generic Mapping Tools, https://www.generic-mapping-tools.org/). (For interpretation of the colors in the figure(s), the reader is referred to the web version of this article.)

been ascribed to inputs from terrigenous sediments and/or sediment melts (König et al., 2016). Although alternative explanations of high $\delta^{98/95}$Mo in arc lavas have also been proposed (Voegelin et al., 2014; Wille et al., 2018), it has been generally suggested that isotopically heavy Mo tends to be selectively incorporated in fluid phases when slabs devolatilize during subduction, while the isotopically light Mo is sequestered in residual rutile within the slab (Freymuth et al., 2015; König et al., 2016; Willbold and Elliott, 2017; Skora et al., 2017). These fractionation effects have been independently confirmed in a more recent study of eclogites in combination with high-pressure experiments (Chen et al., 2019a).

A corollary of these insights into Mo isotope cycling is that ocean crust passing through subduction zones should become isotopically light and carry this distinctive signature into the mantle (Chen et al., 2019a; Freymuth et al., 2015). If subducted ocean crust is important in enriching portions of the convecting upper mantle, as sampled by enriched MORB (E-MORB), then these melts would be expected to inherit such an isotopically light Mo signature. The Mo isotopic study on MORB by Bezard et al. (2016) allowed a preliminary application of this test. In contrast to the scenario outlined above, Bezard et al. (2016) reported E-MORB with Mo slightly isotopically heavier than the majority of normal, depleted MORB (N-MORB). However, the current Mo isotope database for MORB is very small and the possible effects of magma generation and evolution on Mo isotopes remain debated (Bezard et al., 2016; Liang et al., 2017; Voegelin et al., 2014; Wille et al., 2018; Yang et al., 2015). A more comprehensive study of the Mo isotopic compositions of variably enriched MORB is therefore required to implement effectively this novel isotopic test of upper mantle enrichment. Here we present the results of our systematic study on well-characterized MORB samples on and off-axis across morphologically typical ridge segments of the East Pacific Rise (EPR) and seamounts lavas on the flanks of the EPR between 5°N and 12°N (Fig. 1). Our new results, together with existing data, are used to assess the effects of MORB melt generation and evolution on Mo isotopes and the nature of mantle heterogeneity beneath the eastern Pacific.

2. Samples

We report Mo elemental and isotope compositions for twenty-two MORB samples collected by dredging along two traverses across the East Pacific Rise (EPR) axis at 10°30'N and 11°20'N during the Phoenix 02 (R/V Melville) expedition (Batiza et al., 1996) and eight seamount lavas sampled by dredging during the 1988 Raitt 02 expedition aboard R/V Thomas Washington (Fig. 1) (Batiza et al., 1990). Samples from EPR 10°30'N are from 40 dredges out to 50 km from the EPR axis on both the Pacific and Cocos Plates (Fig. 1). Most off-axis samples were dredged from fault scarps, but closer to the ridge axis, an additional 30 samples were recovered by a rock-coring technique, which allowed denser sampling (∼2 samples/km^2) of an area of ∼12 km^2 within ∼3 km of the ridge axis (Regelous et al., 1999). Samples from EPR 10°30'N are more normal, depleted MORB, which are derived from a compositionally uniform source in terms of radiogenic isotopes but span a wide compositional range in MgO (1.8–7.4 wt.%) with well-defined liquid lines of descent (LLD) (Regelous et al., 1999). Temporal changes in major element chemistry have been observed in these lavas, which were interpreted to reflect changes in the average rate of supply of melt to the ridge axis during this period (Regelous et al., 1999). These lavas also show systematic Fe isotopic variation resulting from varying extent of fractional crystallization (Chen et al., 2019b). During early crystallization of olivine, pyroxene and plagioclase, Fe contents and ^{56}Fe/^{54}Fe ratios increase until Fe-Ti oxides appear on the liquidus and begin to crystallize, resulting in a rapid decrease in FeO^t and TiO$_2$ content and a slight decrease in ^{56}Fe/^{54}Fe in residual melts (Chen et al., 2019b).

In contrast, the location at EPR 11°20'N (Fig. 1) is marked by an anomalously large number of enriched MORB (Niu et al., 1999). The seamount lavas are more diverse than axial MORB in composition, varying from highly enriched alkali basalts to extremely depleted tholeiites (Niu et al., 2002). Previous studies showed that radiogenic isotopes such as Sr-Nd-Pb isotope and stable Fe isotopes of these seamount lavas correlated with each other, with the abundances and ratios of incompatible elements, and suggested that their mantle source had long-term lithological heterogeneities on very small scales (Niu et al., 2002; Sun et al., 2020). All studied samples provide sufficient material to allow strict hand-picking of pristine glasses under a binocular microscope.

3. Analytical methods

3.1. Mo isotope measurements

For all the samples analyzed, the glasses were crushed into ∼1 mm fragments and hand-picked under a binocular microscope to select the freshest and mineral-free material. Chemical protocols and data reduction are largely based on those by Willbold et al. (2016). Briefly, sample fragments were cleaned with Milli-Q water for 10 min, three times, in an ultrasonic bath before digestion. For each sample, between 50 and 400 mg of glass fragments were weighed into 50 ml Savillex beakers and spiked with a mixed ^{97}Mo-^{100}Mo tracer to correct for possible mass fractionation occurring during chemical separation and mass spectrometric analysis. For each 50 mg of spiked samples, 1 ml reverse aqua regia (HNO_3:HCl = 3:1) and 0.5 ml HF were added in the beaker, which was then placed on a hotplate at 140 °C for 15 to 48 hrs. Sample solutions were then evaporated to incipient dryness and re-dissolved in 6 M HCl until a clear solution was obtained. Molybdenum was separated from the sample matrix by a single pass column using an Eichrom 100-200 mesh AG1 × 8 anion exchange resin. After chemical separation, samples were analyzed using a multi-collector inductively coupled plasma mass-spectrometer (MC-ICPMS; Nu plasma II) in the Laboratory of Ocean Lithosphere and Mantle Dynamics, Institute of Oceanology, Chinese Academy of Sciences (IOCAS), aspirated as a 50-70 ng/g Mo solution in 0.4M HNO_3-0.05M HF. In order to correct for isobaric interferences of ruthenium (Ru) on masses 98 and 100, we monitored ^{99}Ru as well as ^{101}Ru in the course of analysis with the following cup configuration: ^{94}Mo-^{94}Zr-L4, ^{95}Mo-L3, ^{96}Mo-^{96}Zr-^{96}Ru-L2, ^{97}Mo-L1, ^{98}Mo-^{98}Ru-AX, ^{99}Ru–H1, ^{100}Mo-^{100}Ru-H2, ^{101}Ru–H3. Previous work suggested that there is occasionally a non-Ru contribution to the small signal on mass 99, likely due to polyatomic ions (e.g., $^{64}Zn^{35}Cl$, $^{40}Ar_2^{19}F$), which would lead to an over-correction for the interference (Chen et al., 2019a). To avoid such artefacts, potential Ru interferences were corrected by both ^{99}Ru and ^{101}Ru for comparison, and data were rejected when the 'Ru correction' was more than 0.1‰ in $\delta^{98/95}$Mo. Previous double-spiked Mo work observed that average compositions of the reference standard within a measurement session often deviate slightly from zero (Hin et al., 2013). A correction was made for such drift by subtracting the average composition of NIST SRM 3134 in a measurement session from each sample analysis in the same session.

Replicate digestions and measurements of geological reference materials W-2a yielded $\delta^{98/95}\text{Mo} = -0.05 \pm 0.05$‰ ($n = 9$, 2SD), [Mo] = 0.46 ± 0.06 µg/g, AGV-2 yielded $\delta^{98/95}\text{Mo} = -0.17 \pm 0.03$‰ ($n = 12$, 2SD), [Mo] = 1.98 ± 0.03 µg/g, and BHVO-2 yielded $\delta^{98/95}\text{Mo} = -0.08 \pm 0.04$‰ ($n = 6$, 2SD), [Mo] = 3.57 ± 1.00 µg/g. The isotopic compositions and concentrations of Mo of these geological reference materials agree within error with previously published values (Burkhardt et al., 2014; Chen et al., 2019a; Freymuth et al., 2015; Gaschnig et al., 2017; König et al., 2016; Li et al., 2019; McCoy-West et al., 2019; Willbold et al., 2016; Wille et al., 2018). The total procedural blanks are less than 0.3 ng, which are negligible for the samples.

4. Results

The $\delta^{98/95}$Mo of our samples vary between −0.23‰ and −0.06‰, which is at least three times the long-term reproducibility (better than 0.05‰) (Fig. 2A; Table 1). The calculated reduced χ^2 (or MSWD, Mean Square Weighted Deviation) for our samples is 7.5, which is outside the 95% confidence interval of 0.55 to 1.58 for $n - 1 = 29$ degree of freedom, indicating the dispersion in $\delta^{98/95}$Mo of our samples cannot be adequately explained by analytical uncertainties. The N-MORB samples from EPR 10°30'N have limited variation of $\delta^{98/95}$Mo with an average of -0.20 ± 0.04‰ ($n = 10$, 2SD). In contrast, samples from EPR 11°20'N and seamounts exhibit large variations both in Mo concentration (0.07 to 3.02 µg/g) and $\delta^{98/95}$Mo (−0.23‰ to −0.06‰). The $\delta^{98/95}$Mo of our samples show no correlation with indicators of magma differentiation (e.g., MgO; Fig. 2A). Instead, we observe significant correlations of $\delta^{98/95}$Mo with a series of conventional elemental and isotopic indicators of enrichment both in our samples and most literature data (Fig. 3). Two previously reported MORB samples have much higher $\delta^{98/95}$Mo (Bezard et al., 2016) that are outside of any systematics defined by other seafloor samples (see Supplementary Fig. S1), we exclude these two anomalous samples in the following discussion.

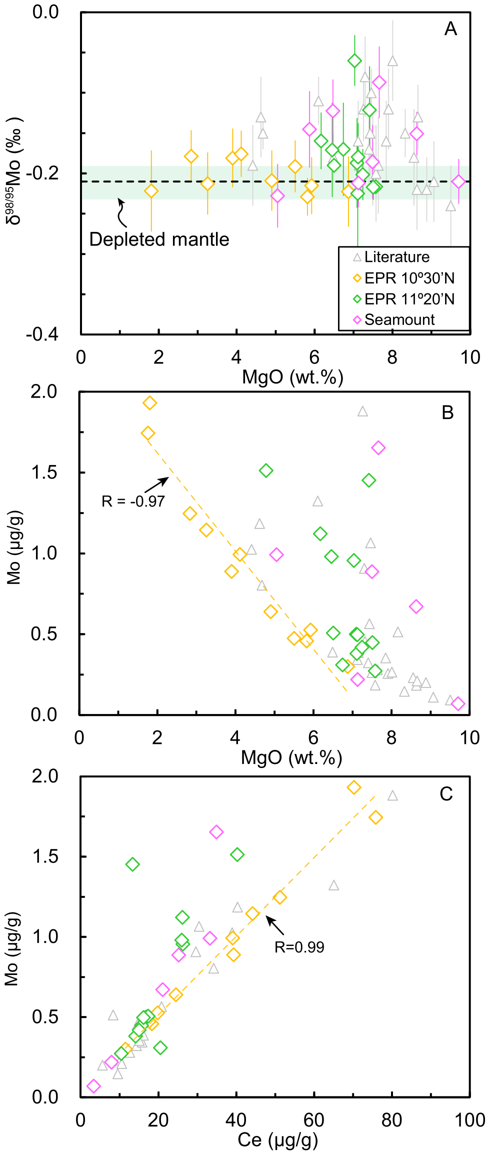

Fig. 2. $\delta^{98/95}$Mo vs. MgO (A), Mo vs. MgO (B) and Mo vs. Ce (C). Light green band shows Mo isotope composition of depleted mantle ($\delta^{98/95}\text{Mo} = -0.21 \pm 0.02$‰; Willbold and Elliott, 2017). Literature data is from Bezard et al. (2016).

5. Discussion

Given stable isotopic variations can be caused by a range of processes, it is crucial to carefully assess processes that may have caused the observed variations of these isotopes, including assimilation of shallow crustal materials during magma ascent, fractional crystallization, partial melting, and addition of recycled materials to the mantle source region.

5.1. The effect of assimilation on Mo isotope systematics

It has been shown that the top few hundred metres of the ocean crust have a $\delta^{98/95}$Mo and Mo/Ce value significantly higher than its lower sections, indicating incorporation of isotopically heavy, seawater-derived Mo into the upper crust during seafloor alteration (Freymuth et al., 2015). Assimilation of altered ocean crust (AOC) could increase $\delta^{98/95}$Mo but should have little ef-

Table 1
Mo isotopes of MORB glasses and seamount lavas from East Pacific Rise at 5°N to 12°N.

Sample	Latitude (°N)	Longitude (°W)	$\delta^{98/95}$Mo (‰)	2SD/2SE	N	Mo (μg/g)	MgO	$(La/Sm)_N$	$^{143}Nd/^{144}Nd$
MORB glasses from East Pacific Rise at 11°20'N									
PH84-1	11.41	103.53	−0.19	0.06	3	0.50	7.09	0.92	0.513127
PH88-1	11.38	103.59	−0.22	0.07	3	0.38	7.11	0.71	0.513147
PH90-2	11.37	103.64	−0.16	0.04	3	1.12	6.17	1.35	0.513103
PH91-1	11.38	103.66	−0.22	0.01	3	0.27	7.58	0.69	0.513159
PH92-1	11.38	103.68	−0.06	0.03	1	0.96	7.03	1.39	0.513078
PH93-6	11.38	103.69	−0.22	0.02	3	0.45	7.51	0.86	0.513190
PH94-1	11.37	103.71	−0.12	0.05	3	1.45	7.42	0.94	0.513105
PH100-1	11.36	103.68	−0.19	0.01	3	0.51	6.50	0.85	0.513133
Replicate			−0.18	0.05	1	0.52			
PH102-1	11.36	103.78	−0.20	0.03	3	0.42	7.24	0.81	0.513145
PH104-1	11.34	103.78	−0.18	0.04	3	0.50	7.12	0.89	0.513162
PH108-1	11.34	103.79	−0.17	0.06	2	0.98	6.46	1.47	0.513053
MORB glasses from East Pacific Rise at 10°30'N									
PH43-2	10.52	103.32	−0.22	0.05	3	1.93	1.81	0.91	0.513142
Replicate			−0.22	0.03	3	1.93			
PH45-2	10.54	103.36	−0.21	0.04	3	1.14	3.25	0.79	0.513147
PH54-1	10.50	103.51	−0.22	0.04	3	0.30	6.87	0.60	0.513163
PH60-6	10.48	103.60	−0.21	0.04	3	0.64	4.90	0.71	0.513147
PH66-1	10.48	103.65	−0.22	0.04	3	0.53	5.92	0.65	0.513158
PH77-7	10.43	103.85	−0.23	0.02	3	0.46	5.82	0.67	0.513158
PH78-1	10.43	103.86	−0.18	0.03	3	1.25	2.83	0.87	0.513166
PH78-2	10.43	103.86	−0.18	0.04	1	0.89	3.90	0.80	0.513155
PH78-5	10.43	103.86	−0.18	0.03	3	0.99	4.11	0.79	0.513172
PHGC-74	10.50	103.62	−0.19	0.03	3	0.47	5.50	0.69	0.513140
Seamount lavas near-EPR between 5°N and 12°N									
R13-1	8.40	104.07	−0.15	0.05	3	3.06	5.87	2.96	0.512956
Replicate			−0.17	0.06	3	3.02			
R15-1	8.76	104.54	−0.12	0.04	3	2.64	6.47	2.91	0.512979
R18-3	8.93	104.46	−0.19	0.05	3	0.89	7.49	1.73	0.513041
R3-1	5.78	102.21	−0.21	0.03	1	0.07	9.70	0.35	0.513183
Replicate			−0.18	0.04	1	0.07			
R32-1	9.09	104.92	−0.15	0.03	3	0.67	8.63	1.57	0.513047
R71-21	10.26	103.74	−0.23	0.04	3	0.99	5.05	0.70	0.513154
R78-6	11.22	103.58	−0.09	0.04	3	1.65	7.66	3.73	0.512970
R8-8	8.34	103.06	−0.21	0.03	3	0.22	7.13	0.64	0.513131

Major, trace element concentrations and Nd isotopes are from literature (Chen et al., 2019b; Niu et al., 1999; Sun et al., 2020 and reference therein). Replicate analysis on separate dissolution of the same sample. Uncertainties of $\delta^{98/95}$Mo are given as two standard deviation (2SD, $N > 1$) or two standard error (2SE, $N = 1$), where N refers to number of isotopic analyses using the same solution.

fect on absolute or relative abundances of elements unsusceptible to alteration. Thus, such assimilation cannot account for the correlated trends of $\delta^{98/95}$Mo with $(La/Sm)_N$, Nb/La, Nb/Zr and Th/Yb (Fig. 3A–D). Moreover, although seafloor alteration can affect Sr isotopes, it cannot change Nd isotopes, thus assimilation of AOC cannot account for the negative trend between $\delta^{98/95}$Mo and $^{143}Nd/^{144}Nd$ (Fig. 3E). Thus, isotopically heavy Mo cannot be caused by assimilation of Mo-rich material at shallow levels.

5.2. The effect of fractional crystallization on Mo isotope systematics

Bezard et al. (2016) showed no correlation of $\delta^{98/95}$Mo with indices of magma differentiation for MORB from the Pacific-Antarctic ridge and the Mohns-Knipovich ridge and suggested negligible Mo isotope fractionation during MORB magma evolution (Bezard et al., 2016). Although MORB glasses from Bezard et al. (2016) show a wide range in MgO (4.4–9.5wt.%), they are not cogenetic. MORB glasses from EPR 10°30'N in our study are ideal samples to study possible effects of magma evolution on Mo isotope fractionation at ocean ridges as these samples are derived from a compositionally uniform source in terms of radiogenic isotopes and incompatible elements but span a wide compositional range in MgO (1.8 to 7.4 wt.%; Fig. 2A) with well-defined liquid lines of descent (LLD) (Chen et al., 2019b; Regelous et al., 1999).

As shown in Fig. 2B, Mo concentrations in MORB glasses from EPR 10°30'N correlate well with various magmatic differentiation indicators (e.g., MgO). Our 10°30'N data further show that Mo and Ce are similarly incompatible during magma evolution (Fig. 2C), in keeping with the nearly constant Mo/Ce (∼0.03) in seafloor basalts (Newsom et al., 1986). In contrast, Mo concentrations in MORB glasses from EPR 11°20'N and seamounts show a wide range at given MgO or Ce (Fig. 2B–C), reflecting their source heterogeneity. The significant ($R = -0.97$) linear Mo-MgO correlation defined by EPR 10°30'N samples (Fig. 2B) indicates that Mo is likely incompatible in all the liquidus phases (i.e., olivine, plagioclase, clinopyroxene and magnetite/ilmenite) during MORB melt evolution, and that none of these phases are important hosts for Mo. Thus, the effect of fractionation of these liquidus phases on the magma $\delta^{98/95}$Mo is likely insignificant. This is confirmed by the observation that $\delta^{98/95}$Mo of EPR 10°30'N samples is constant and is independent of MORB melt evolution shown by the varying MgO (Fig. 2A). Thus, Mo isotope ratios are unfractionated during MORB magma differentiation, consistent with previous inference (Bezard et al., 2016), but contrary to interpretations of some arc-lava suites (Voegelin et al., 2014; Wille et al., 2018). The measured Mo isotope compositions of MORB and seamount samples thus represent those of primitive magmas.

5.3. The effect of mantle melting on Mo isotopes

Before using Mo isotopes of MORB samples to infer their mantle sources, we need to assess the possible effect of mantle melting on Mo isotopes. Based on the absence of correlation between $\delta^{98/95}$Mo and Na_8 (the calculated Na_2O at $MgO = 8$ wt.%; Klein and Langmuir, 1987), Bezard et al. (2016) suggested a negligible effect of mantle melting on Mo isotope variations. In con-

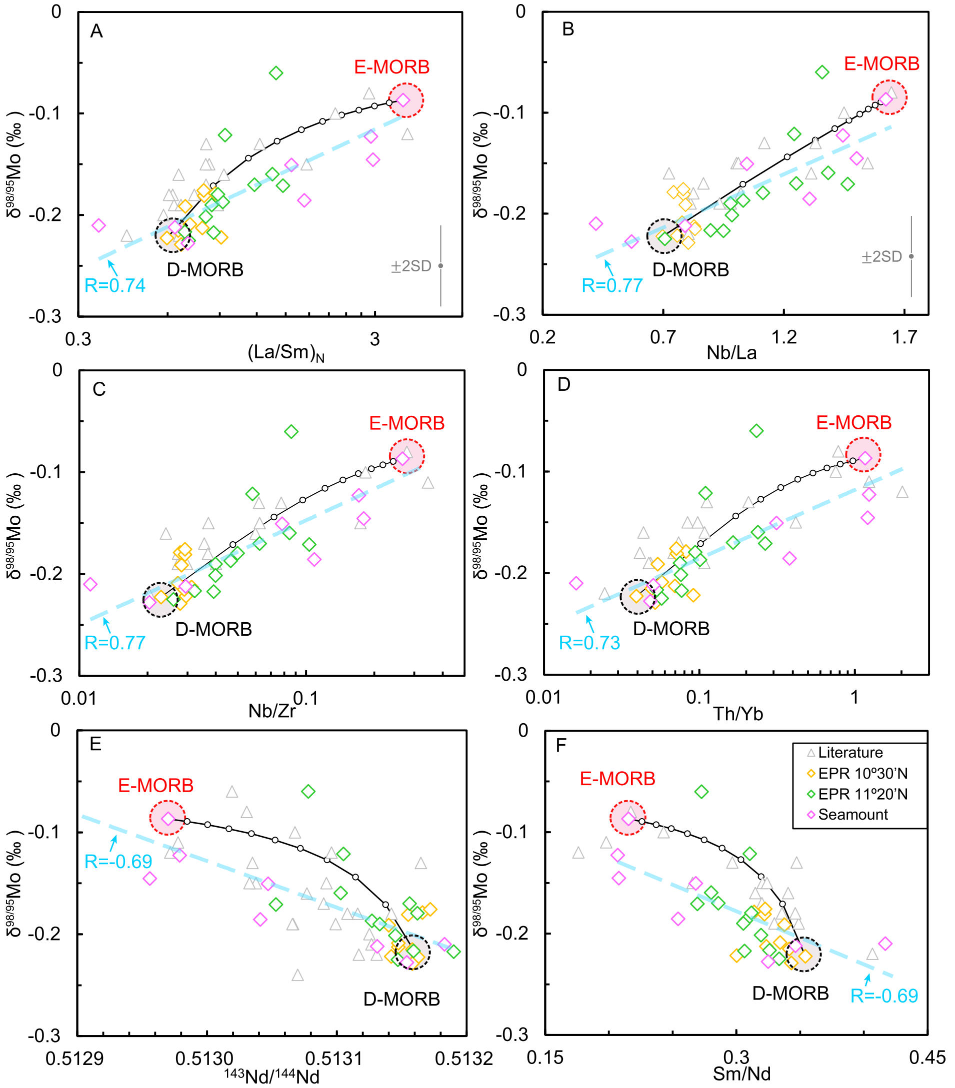

Fig. 3. Variation diagrams of $\delta^{98/95}$Mo against (La/Sm)$_N$ (A), Nb/La (B), Nb/Zr (C), Th/Yb (D), ^{143}Nd/^{144}Nd (E) and Sm/Nd (F). Light blue dash lines are regression lines of our samples. Trace element concentrations of the samples have been reported previously (Chen et al., 2019b; Niu et al., 1999; Sun et al., 2020 and reference therein) and are compiled in Table S1. The mixing lines (black lines) are calculated using the depleted MORB (D-MORB) composition represented by sample PH54-1 and an enriched seamount sample R78-6 as end-member compositions (see Table 1). The mixing lines show that all the isotopic and trace element data can be explained by mixing between an incompatible element depleted end-member MORB melt (i.e., low $\delta^{98/95}$Mo, La/Sm, Nb/La, Nb/Zr, Th/Yb and high Sm/Nd plus high ^{143}Nd/^{144}Nd) and an incompatible element enriched end-member MORB melt (i.e., high $\delta^{98/95}$Mo, La/Sm, Nb/La, Nb/Zr, Th/Yb and low Sm/Nd plus low ^{143}Nd/^{144}Nd). Note that such mixing is an effective approximation using erupted melts which are 100 s of kilometres apart and are of different eruption ages, but the actual "mixing" is melting-induced mixing of compositionally varying sources with enriched lithologies dispersed in the more depleted matrix of varying proportions (Niu et al., 2002). Literature MORB data are from Bezard et al. (2016) with two outliers excluded. The Mo isotope analytical uncertainty is based on repeated analyses of USGS reference rock BHVO-2.

trast, Liang et al. (2017) reported large variations of Mo isotopes in ocean island basalts (OIB; -0.59‰ to $+0.10$‰) that define a broad positive $\delta^{98/95}$Mo-Mo/Ce correlation and a broad negative $\delta^{98/95}$Mo-La/Yb correlation. They thus suggested that Mo isotopes are fractionated by low degrees of mantle melting, resulting from an oxide or a residual sulfide liquid selectively incorporating isotopically heavy Mo in the mantle relative to the melt (Liang et al., 2017). According to such a model, lower degree melting would produce melts with higher Mo/Cu and lower $\delta^{98/95}$Mo (Li et al., 2019) as Cu is more strongly partitioned into sulfides than Mo (Li and Audétat, 2012). However, this is not observed in our samples (Supplementary Fig. S2).

Recently, McCoy-West et al. (2019) constructed a non-modal batch melting model with theoretically estimated Mo isotope fractionation factors and inferred that Mo isotopes can be significantly fractionated ($\Delta^{98/95}\text{Mo}_{\text{melt-solid}} > 0.1$‰) during partial melting of the mantle. This fractionation is driven by Mo^{6+} species being isotopically heavier and significantly more incompatible than Mo^{4+}, leading to a melt with higher Mo^{6+}/ΣMo and $\delta^{98/95}$Mo than the residue (McCoy-West et al., 2019). The fractionation between melt and original mantle source would be greater for smaller degrees of melting and/or under more reduced conditions (McCoy-West et al., 2019). In order to quantitatively show the effects of mantle melting on Mo isotopes of the melt, we model the behavior of Mo isotopes during mantle melting using non-modal batch melting models similar to those from McCoy-West et al. (2019) (see Supplementary Table 2 for parameters). Previous work suggested that the range in the degree of partial melting during the production of MORB varies from 10% to 20% (e.g., Niu, 1997), which alone would produce no more than 0.07‰ isotopic variation of $\delta^{98/95}$Mo even at reduced conditions with Mo^{6+}/ΣMo of 0.9 (Fig. 4A). This is insufficient to explain the variation of $\delta^{98/95}$Mo in our samples. Moreover, modern mantle is thought to be more oxidized (Mo^{6+}/ΣMo ≈ 0.99) (McCoy-West et al., 2019), indicating the fractionation of Mo isotopes should be smaller. Thus, we conclude that

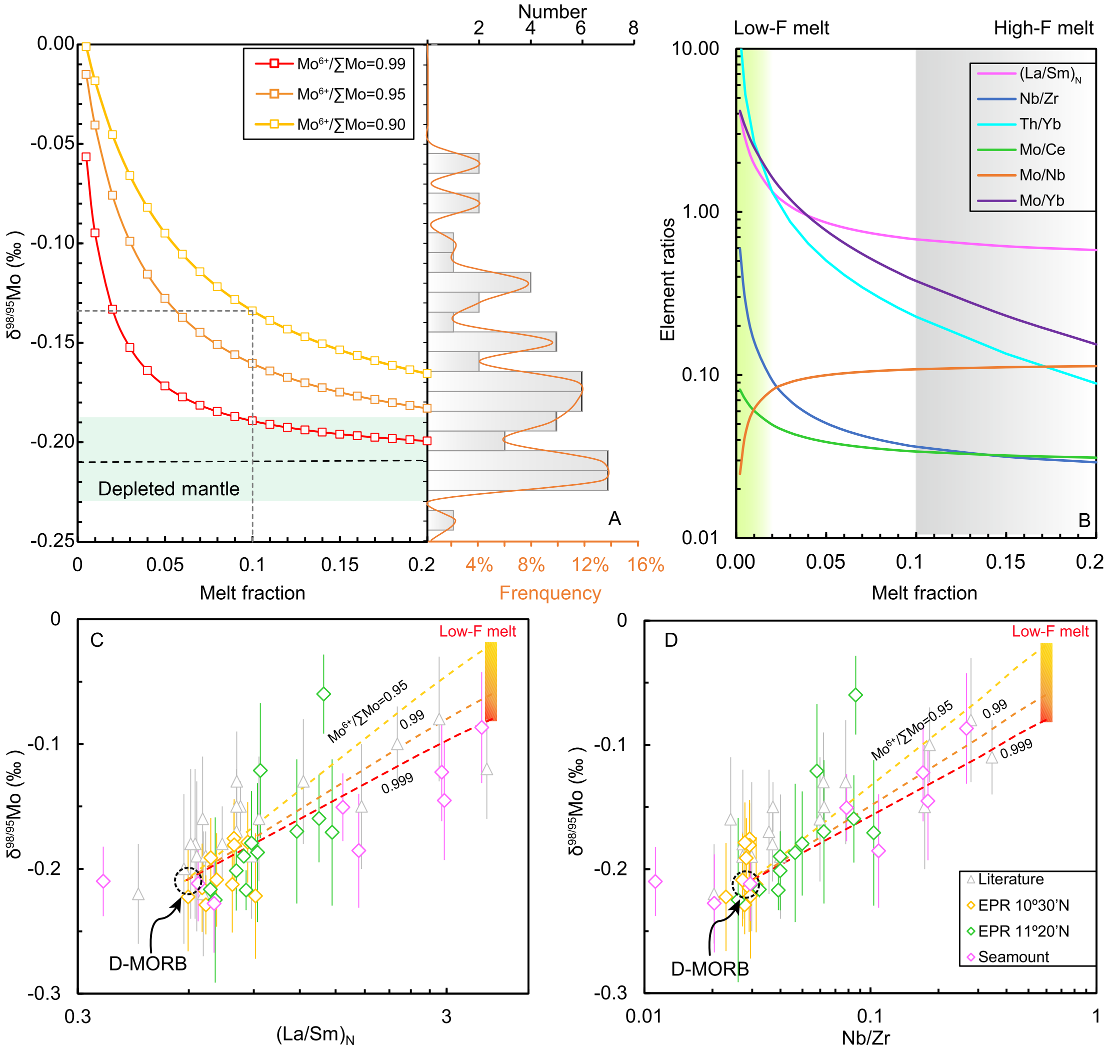

Fig. 4. Non-modal batch melting modelling on both incompatible trace element ratios and Mo isotope composition of melt. Variations of $\delta^{98/95}$Mo (A), $(La/Sm)_N$, Nb/Zr, Th/Yb, Mo/Ce, Mo/Nb and Mo/Yb ratios (B) in melts as a function of the extent of melting of depleted mantle compositions at different mantle fO_2 ($Mo^{6+}/\sum Mo$ = 0.999 to 0.95). (C-D) display mixing lines between D-MORB (represented by 20% melting of DMM) and low degree melts generated by 0.2% melting of mantle at different mantle fO_2 ($Mo^{6+}/\sum Mo$ = 0.999 to 0.95). Literature MORB data are from Bezard et al. (2016) with two outliers excluded. The partial-melting model was calculated at a constant temperature (1300 °C). The green band in A shows Mo isotope composition of depleted mantle (Willbold and Elliott, 2017). The histogram and orange line in A on the right hand axis is the distribution (bin width = 0.01‰, N = 55) and frequency curve of $\delta^{98/95}$Mo of measured MORB glasses and seamount lavas from this study and Bezard et al. (2016) without the two outliers.

partial melting of a peridotite mantle during MORB melt generation cannot explain the Mo isotope variation of our samples.

5.4. Molybdenum isotope composition of depleted upper mantle

As discussed above, Mo isotopes are unlikely to be significantly fractionated during MORB magma generation and evolution, indicating that the Mo isotope composition of MORB samples can be used to discuss their mantle source. In our study, the N-MORB glasses from EPR 10°30'N display uniform $\delta^{98/95}$Mo values with a mean of $-0.204 \pm 0.013‰$ ($2SD/\sqrt{n}$, n = 10, Fig. 2A), which is identical to that of previous estimates of the depleted mantle (e.g., Bezard et al., 2016; Freymuth et al., 2015). Notably, this value is also similar to the averages for Phanerozoic Gorgona komatiites ($\delta^{98/95}Mo = -0.207 \pm 0.034‰$), the parental melt of Baffin Island picrites ($\delta^{98/95}Mo = -0.210 \pm 0.010‰$; McCoy-West et al., 2019) and mantle xenoliths from Kilbourne Hole, Tariat and Vitim ($\delta^{98/95}Mo = -0.22 \pm 0.06‰$, n = 13, 95% CI; Liang et al., 2017). Thus, our study reaffirms the estimation that depleted mantle has a sub-chondritic $\delta^{98/95}$Mo value ($-0.21 \pm 0.02‰$) (Willbold and Elliott, 2017).

5.5. Origin of Mo isotope variation in MORB and seamount lavas

Given that the $\delta^{98/95}$Mo variations observed in the MORB and seamount samples are unlikely caused by processes of magma generation and evolution, they must largely reflect compositional variations in the mantle source regions, indicating that mantle heterogeneities exert the primary control over the observed Mo isotope variations. The significant correlations of Mo isotope composition with commonly used indices of mantle enrichment (Fig. 3) indicate that our new samples and literature data approximate to two-component mixing between a depleted endmember with low $\delta^{98/95}$Mo (∼−0.21‰), La/Sm, Nb/La, Nb/Zr and Th/Yb, and high Sm/Nd and $^{143}Nd/^{144}Nd$, and an enriched endmember with high $\delta^{98/95}$Mo (∼−0.05‰), La/Sm, Nb/La, Nb/Zr and Th/Yb, and low Sm/Nd and $^{143}Nd/^{144}Nd$ (Fig. 3). Mechanistically we envisage mixing of melts to produce the range of magma compositions seen, but the endmember melt compositions in turn reflect variable mantle sources.

To test the likelihood of the two-component mixing scenario, we have calculated binary mixing curves between incompatible element and Mo isotope compositions using a depleted end-member

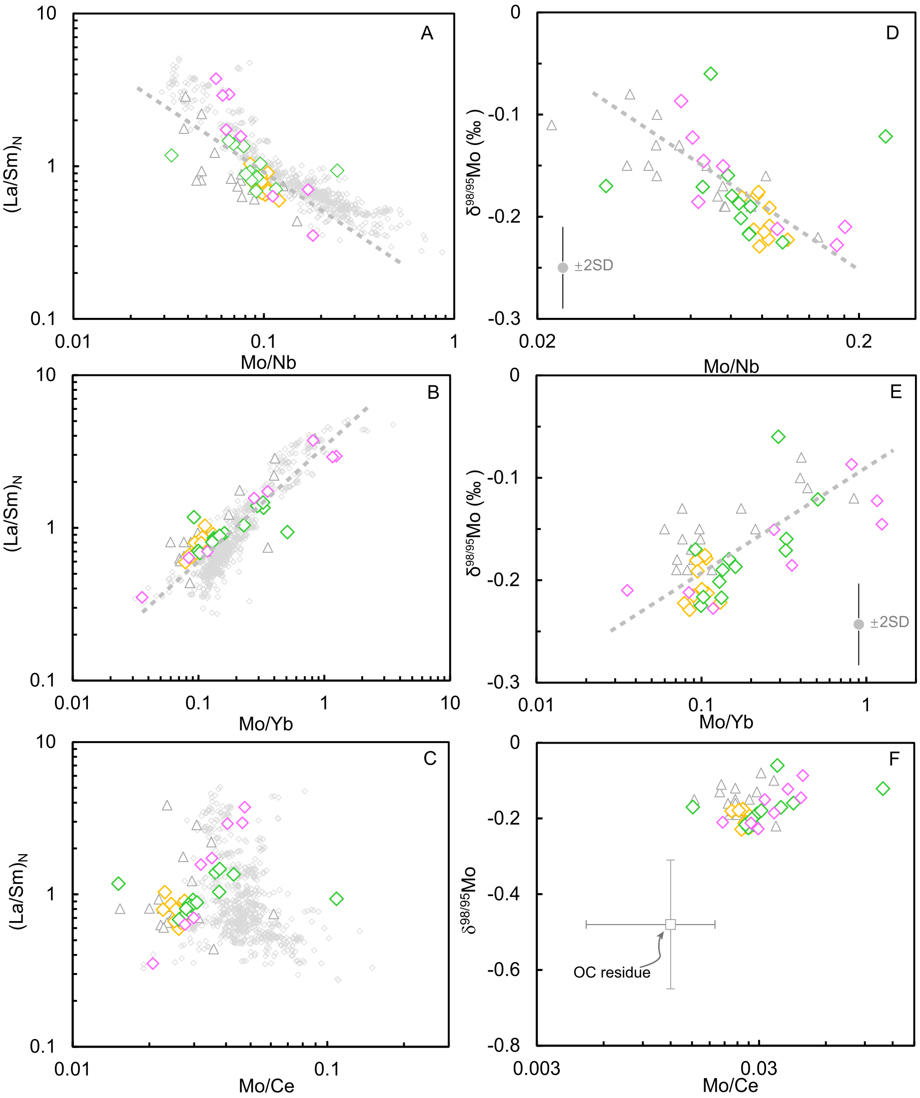

Fig. 5. Variation diagrams of $(La/Sm)_N$ against Mo/Nb (A), Mo/Yb (B), Mo/Ce (C), and $\delta^{98/95}$Mo against Mo/Nb (D), Mo/Yb (E), Mo/Ce (F). Plotted also are literature MORB data (cycles; Jenner and O'Neill, 2012; Kamenetsky and Eggins, 2012; Sun et al., 2003). Ocean crust (OC) residues are average value (±SD) of eclogites and blueschists from Chen et al. (2019a) and reference therein. Other symbols are the same as in Fig. 2.

composition represented by sample PH54-1 and an enriched one represented by sample R78-6. The resulting mixtures reasonably well match the trends between Mo isotope ratios and incompatible element ratios and Nd isotopes (Fig. 3). Our model uses compositions of melts which were erupted 100 s of kilometres apart and at different times, but this more generally represents the net effect of melting a depleted mantle matrix that variably contains a dispersed enriched lithology (Niu et al., 2002).

The exact time and place where these two endmembers were physically juxtaposed is not constrained. However, the unradiogenic Nd isotope compositions of the enriched component and the covariation of Sm/Nd and $\delta^{98/95}$Mo with ^{143}Nd/^{144}Nd (Fig. 3E&F) indicate both endmembers must be ancient and their trace element and isotopic characteristics have independently developed for some time (>1 Ga) (Niu et al., 2002). This is also supported by covariations of ^{87}Sr/^{86}Sr and Rb/Sr as well as ^{206}Pb/^{204}Pb and U/Pb with $\delta^{98/95}$Mo (Fig. S3) in our samples, most strikingly for the seamount samples. While there is some variability in Rb/Sr unrelated to ^{87}Sr/^{86}Sr for the 10°30'N samples, and to a lesser extent U/Pb variability relative to ^{206}Pb/^{204}Pb, this is evidently a consequence of magmatic differentiation (see Fig S3). In summary, the Mo isotope variations of EPR MORB and seamount samples require incorporation of a recycled, enriched component with heavier Mo into the ambient depleted MORB mantle (DMM). In the following, we discuss the mechanisms that might have been responsible for the above processes of mantle enrichment.

5.5.1. Mantle enriched by recycled oceanic crust or sediments?

Recycled oceanic crust (ROC) has long been considered as a candidate for mantle enrichment (e.g., Allègre and Turcotte, 1986; Rehkämper and Hofmann, 1997). However, whether the ancient subducted and recycled ocean crust is chemically and isotopically enriched or not is highly debated (Donnelly et al., 2004; Niu et al., 2002; Thomson et al., 2019). The Mo systematics here can provide an effective diagnostic tool in assessing the above ROC model. Recycled, mafic oceanic crust should have low Mo/Ce ratio (lower than 0.03) as it loses much of Mo during subduction (Chen et al., 2019a; Freymuth et al., 2015), thus it cannot explain the elevated Mo/Ce ratios of E-MORB (Fig. 5F). More importantly, the dehydrated residues of subducted ocean crust (as eclogite) are further argued to be isotopically light in Mo (<−0.20‰) (Fig. 5F; Chen et al., 2019a; Freymuth et al., 2015; Greaney et al., 2018), which is in sharp contrast to the heavy Mo isotope characteristics of the E-MORB. A recent study of adakitic andesites from Tianshan, which

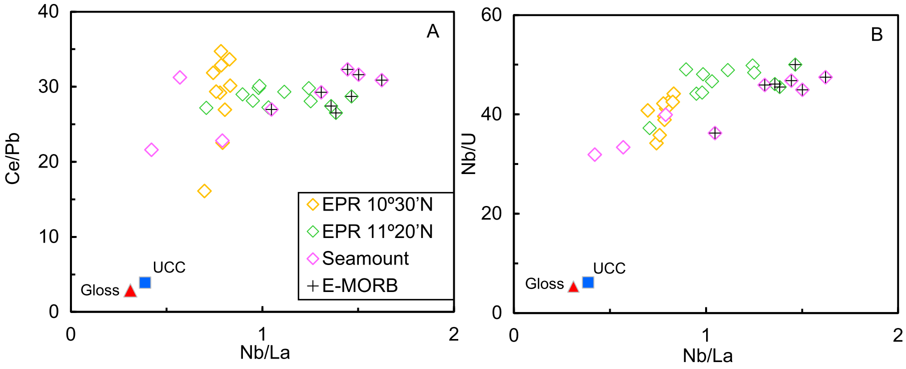

Fig. 6. Variation of Ce/Pb (A) and Nb/U (B) as a function of Nb/La. Composition of Upper Continental Crust (UCC; Rudnick and Gao, 2003) and Global Subducting Sediment (GLOSS; Plank and Langmuir, 1998) are also plotted for comparison. E-MORB (symbols with crosses) are as defined by Batiza et al. (1996) and reference therein.

are suggested to have derived from dehydrated ocean crust, have low $\delta^{98/95}$Mo (-0.48 to -0.27‰) (Zhang et al., 2020), reaffirming that the subducted oceanic crust is most likely depleted in isotopically heavy Mo.

Recycled sediments have also been thought to play a key role in the formation of the E-MORB reservoir (Nielsen et al., 2018; Rehkämper and Hofmann, 1997). However, recycled sediments or continental crustal materials are in general strongly enriched in large ion lithosphile elements (LILE) but depleted in Nb and Ta relative to elements of similar compatibility, thus cannot explain the elevated Ce/Pb, Nb/U and Nb/La ratios in EPR E-MORBs in our study (Fig. 6; Niu et al., 1999; Hofmann et al., 1986), which suggests that there is little sedimentary material in the enriched mantle component.

5.5.2. *Mantle enriched by recycled fluid-modified mantle wedge?*

In a similar set of EPR MORB samples, isotopically heavy Li was found to be associated with geochemical indices of enrichment. These variations were argued to result from a fluid-modified mantle that once overlaid the dehydrating slab, which was enriched during its residence in a subduction zone, and was then mixed back into the upper mantle to result in compositional variability (Elliott et al., 2006). At first glance, such model may also explain the Mo isotope variation in our samples. Isotopically heavy Mo observed in arc lavas (Chen et al., 2019a; Freymuth et al., 2015; König et al., 2016; Villalobos-Orchard et al., 2020) presumably passes through the mantle wedge. Mixing such fluid-modified mantle with depleted mantle may account for the variation of Mo isotopes of the MORB samples. However, there is no known major mineral host for Mo in the mantle wedge, whereas Li readily resides in olivine.

5.5.3. *Mantle enriched by recycled oceanic mantle lithosphere?*

As illustrated in Fig. 5A–C, $(La/Sm)_N$ ratios of our samples and global MORB samples (Jenner and O'Neill, 2012; Kamenetsky and Eggins, 2012; Sun et al., 2003) display a negative correlation with Mo/Nb, a positive correlation with Mo/Yb but no correlation with Mo/Ce, indicating that the elemental incompatibilities exert the primary control on these correlations as $D_{Nb} < D_{Mo} \approx D_{Ce} < D_{Yb}$. Notably, $\delta^{98/95}$Mo of our samples and literature MORB samples show similar covariations with Mo/Nb, Mo/Yb and Mo/Ce ratios (Fig. 5D–E). Taking together with the broad correlations of Mo isotopes with incompatible element ratios and radiogenic isotopic ratios (Fig. 3), we suggest that the enriched endmember/lithologies are ultimately of magmatic origin, resulting from low degree melting processes. This is in keeping with previous observations that the correlations of Sr and Nd isotope ratios with the abundances and ratios of incompatible elements in EPR MORB and near-EPR seamount lavas are better for the progressively more incompatible elements, which is best understood in terms of low degree melt enrichment (Niu et al., 2002).

To constrain the effect of low degree melting in generating the enriched endmember, we have conducted combined models of partial melting of the depleted mantle for both incompatible elements and Mo isotope ratios using a non-modal batch melting model following the methods proposed in McCoy-West et al. (2019) as discussed above. Mo isotopic compositions of the DMM are assumed to be $\delta^{98/95}\text{Mo} = -0.21$‰ (see above) and relevant incompatible element concentrations of DMM are from Salters and Stracke (2004). Fig. 4 shows results of the melting model with $\delta^{98/95}$Mo and representative ratios of more-to-less incompatible elements plotted against melt fraction. Low degree melting (<2%) can effectively fractionate both elements with minor differences in incompatibility and Mo isotopes (Fig. 4A–B) while high degree melting (ca. 5% to 20%) has little effect on those element ratios and Mo isotopes (Fig. 4A–B). This reaffirms the above inference that high degree melting for the present-day MORB generation can neither result in significant Mo isotope fractionation of the melt from its source, nor fractionate elements with small differences in incompatibility. In contrast, ~0.2% melting of modern mantle ($\text{Mo}^{6+}/\sum\text{Mo} = 0.99$) yields a melt with much higher $\delta^{98/95}\text{Mo} = -0.02$‰, $(La/Sm)_N = 4.0$, $Nb/La = 2.0$, $Nb/Zr = 0.6$ and $Th/Yb = 12.3$ than its source. Such a low degree melt (low-F melt) has characteristics largely resembling the enriched endmember that was inferred from the mixing trends defined by our samples (Fig. 4C–D). Mixing such low degree melts, generated at variable mantle oxygen fugacity ($\text{Mo}^{6+}/\sum\text{Mo} = 0.95$ to 0.999), with D-MORB can broadly reproduce Mo isotope ratios and incompatible element ratios of the MORB and seamount lavas (Fig. 4C–D). This suggests that the enriched endmember is most likely volumetrically small lithologies formed by low degree melts in the past and dispersed in the compositionally depleted peridotitic matrix.

Several studies have proposed that the enriched low degree melt can be readily frozen and incorporated as 'metasomatic' dikes or veins in the thickening oceanic lithosphere at the low velocity zone (LVZ)-lithosphere interface (Green and O'Hara, 1971; Green and Liebermann, 1976; Niu and O'Hara, 2003; Niu et al., 2002). Such metasomatized oceanic lithosphere materials will be mixed back into the upper mantle over much of Earth's history by subduction and will result in mantle compositional heterogeneities, accounting for the enriched characters of E-MORB. Our new findings thus provide important, new evidence for recycled oceanic lithosphere in generating chemical heterogeneity in the upper mantle.

6. Conclusion

Mo isotopes of MORB from the East Pacific Rise (EPR) and near-EPR seamounts show significant Mo isotope variations, ranging from −0.23‰ to −0.06‰. The absence of correlation of Mo isotope variations of MORB in our study across a wide range of magmatic differentiation and calculations of the effect of high degrees of melting suggest that Mo isotopes are unlikely to be fractionated during MORB melt generation and evolution. Taking together with the literature data, we show that MORB Mo isotope compositions vary systematically with a set of indices of mantle enrichment, which most likely results from two-component mixing between an incompatible element depleted endmember with low $\delta^{98/95}$Mo (∼−0.21‰) and an incompatible element enriched endmember with high $\delta^{98/95}$Mo (∼−0.05‰). The association of heavier Mo isotopic compositions with the more enriched MORB cannot be explained by recycled ocean crust with or without sediment being the enriched endmember. Instead, our new data and modelling indicate that the enriched endmember is most consistent with localized low degree melt enrichment (metasomatism) within the depleted MORB mantle most likely at the lithosphere-asthenosphere boundary (LAB) in Earth's history. We thus provide new evidence that recycled oceanic mantle lithosphere, metasomatized by low degree melt plays a key role in the formation of E-MORB source lithologies.

CRediT authorship contribution statement

Shuo Chen: Conceptualization, Investigation, Methodology, Data curation, Funding acquisition, Original draft preparation. **Pu Sun**: Investigation, Methodology, Writing–review & editing. **Yaoling Niu**: Conceptualization, Supervision, Resources, Funding acquisition, Writing–review & editing. **Pengyuan Guo**: Investigation, Methodology, Review & editing. **Remco Hin**: Methodology, Modelling, Review & editing. **Tim Elliott**: Conceptualization, Supervision, Writing–review & editing.

Declaration of competing interest

The authors declare that they have no known competing financial interests or personal relationships that could have appeared to influence the work reported in this paper

Acknowledgements

We thank Hongmei Gong and Xiaohong Wang for the laboratory assistance and Dr. Paolo A. Sossi for using his melting models. We are also grateful to Yanhong Chen and Cuilin Li for helping to generate Fig. 1. The constructive comments by Dr. Godfrey Fitton and two anonymous reviewers and the editorial handling by Dr. Laurence Coogan are gratefully acknowledged. This work was funded by the National Natural Science Foundation of China (NSFC) grants (41906050, 41630968, 9195821), NSFC-Shandong Joint Fund for Marine Science Research Centers grant (U1606401), and grants of Youth Innovation Promotion Association, Chinese Academy of Sciences (2021206) and the 111 Project (B18048).

Appendix A. Supplementary material

Supplementary material related to this article can be found online at https://doi.org/10.1016/j.epsl.2021.117283.

References

Allègre, C.J., Turcotte, D.L., 1986. Implications of a two-component marble-cake mantle. Nature 323, 123–127.

Andersen, M.B., Elliott, T., Freymuth, H., Sims, K.W., Niu, Y., Kelley, K.A., 2015. The terrestrial uranium isotope cycle. Nature 517, 356–359.

Batiza, R., Niu, Y., 1992. Petrology and magma chamber processes at the East Pacific Rise ∼9°30′N. J. Geophys. Res., Solid Earth 97, 6779–6797.

Batiza, R., Niu, Y., Zayac, W.C., 1990. Chemistry of seamounts near the East Pacific Rise: implications for the geometry of subaxial mantle flow. Geology 18, 1122–1125.

Batiza, R., Niu, Y., Karsten, J., Boger, W., Potts, E., Norby, L., Butler, R., 1996. Steady and non-steady state magma chambers below the East Pacific Rise. Geophys. Res. Lett. 23, 221–224.

Bezard, R., Fischer-Gödde, M., Hamelin, C., Brennecka, G.A., Kleine, T., 2016. The effects of magmatic processes and crustal recycling on the molybdenum stable isotopic composition of Mid-Ocean Ridge Basalts. Earth Planet. Sci. Lett. 453, 171–181.

Burkhardt, C., Hin, R.C., Kleine, T., Bourdon, B., 2014. Evidence for Mo isotope fractionation in the solar nebula and during planetary differentiation. Earth Planet. Sci. Lett. 391, 201–211.

Chen, S., Hin, R.C., John, T., Brooker, R., Bryan, B., Niu, Y., Elliott, T., 2019a. Molybdenum systematics of subducted crust record reactive fluid flow from underlying slab serpentine dehydration. Nat. Commun. 10, 4773.

Chen, S., Niu, Y., Guo, P., Gong, H., Sun, P., Xue, Q., Duan, M., Wang, X., 2019b. Iron isotope fractionation during mid-ocean ridge basalt (MORB) evolution: evidence from lavas on the East Pacific Rise at 10°30′N and its implications. Geochim. Cosmochim. Acta 267, 227–239.

Donnelly, K.E., Goldstein, S.L., Langmuir, C.H., Spiegelman, M., 2004. Origin of enriched ocean ridge basalts and implications for mantle dynamics. Earth Planet. Sci. Lett. 226, 347–366.

Elliott, T., Thomas, A., Jeffcoate, A., Niu, Y., 2006. Lithium isotope evidence for subduction-enriched mantle in the source of mid-ocean-ridge basalts. Nature 443, 565–568.

Freymuth, H., Vils, F., Willbold, M., Taylor, R.N., Elliott, T., 2015. Molybdenum mobility and isotopic fractionation during subduction at the Mariana arc. Earth Planet. Sci. Lett. 432, 176–186.

Gaschnig, R.M., Reinhard, C.T., Planavsky, N.J., Wang, X., Asael, D., Chauvel, C., 2017. The molybdenum isotope system as a tracer of slab input in subduction zones: an example from Martinique, Lesser Antilles Arc. Geochem. Geophys. Geosyst. 18, 4674–4689.

Greaney, A.T., Rudnick, R.L., Romaniello, S.J., Anbar, A.D., 2018. Completing the molybdenum isotope mass balance in subduction zones. In: Goldschmidt Abstracts.

Green, D., O'Hara, M., 1971. Composition of basaltic magmas as indicators of conditions of origin: application to oceanic volcanism. Philos. Trans. R. Soc. Lond. Ser. A, Math. Phys. Sci., 707–725.

Green, D.H., Liebermann, R.C., 1976. Phase equilibria and elastic properties of a pyrolite model for the oceanic upper mantle. Tectonophysics 32, 61–92.

Hin, R.C., Burkhardt, C., Schmidt, M.W., Bourdon, B., Kleine, T., 2013. Experimental evidence for Mo isotope fractionation between metal and silicate liquids. Earth Planet. Sci. Lett. 379, 38–48.

Hofmann, A.W., 1997. Mantle geochemistry: the message from oceanic volcanism. Nature 385, 219.

Hofmann, A.W., Jochum, K.P., Seufert, M., White, W.M., 1986. Nb and Pb in oceanic basalts: new constraints on mantle evolution. Earth Planet. Sci. Lett. 79, 33–45.

Jenner, F.E., O'Neill, H.S.C., 2012. Analysis of 60 elements in 616 ocean floor basaltic glasses. Geochem. Geophys. Geosyst. 13.

Kamenetsky, V.S., Eggins, S.M., 2012. Systematics of metals, metalloids, and volatiles in MORB melts: effects of partial melting, crystal fractionation and degassing (a case study of Macquarie Island glasses). Chem. Geol. 302–303, 76–86.

Klein, E.M., Langmuir, C.H., 1987. Global correlations of ocean ridge basalt chemistry with axial depth and crustal thickness. J. Geophys. Res. 92, 8089.

König, S., Wille, M., Voegelin, A., Schoenberg, R., 2016. Molybdenum isotope systematics in subduction zones. Earth Planet. Sci. Lett. 447, 95–102.

Li, H.-Y., Li, J., Ryan, J.G., Li, X., Zhao, R.-P., Ma, L., Xu, Y.-G., 2019. Molybdenum and boron isotope evidence for fluid-fluxed melting of intraplate upper mantle beneath the eastern North China Craton. Earth Planet. Sci. Lett. 520, 105–114.

Li, Y., Audétat, A., 2012. Partitioning of V, Mn, Co, Ni, Cu, Zn, As, Mo, Ag, Sn, Sb, W, Au, Pb, and Bi between sulfide phases and hydrous basanite melt at upper mantle conditions. Earth Planet. Sci. Lett. 355–356, 327–340.

Liang, Y.-H., Halliday, A.N., Siebert, C., Fitton, J.G., Burton, K.W., Wang, K.-L., Harvey, J., 2017. Molybdenum isotope fractionation in the mantle. Geochim. Cosmochim. Acta 199, 91–111.

McCoy-West, A.J., Chowdhury, P., Burton, K.W., Sossi, P., Nowell, G.M., Fitton, J.G., Kerr, A.C., Cawood, P.A., Williams, H.M., 2019. Extensive crustal extraction in Earth's early history inferred from molybdenum isotopes. Nat. Geosci. 12, 946–951.

Nebel, O., Sossi, P.A., Bénard, A., Arculus, R.J., Yaxley, G.M., Woodhead, J.D., Rhodri Davies, D., Ruttor, S., 2019. Reconciling petrological and isotopic mixing mechanisms in the Pitcairn mantle plume using stable Fe isotopes. Earth Planet. Sci. Lett. 521, 60–67.

Newsom, H., White, W., Jochum, K., Hofmann, A., 1986. Siderophile and chalcophile element abundances in oceanic basalts, Pb isotope evolution and growth of the Earth's core. Earth Planet. Sci. Lett. 80, 299–313.

Nielsen, S.G., Horner, T.J., Pryer, H.V., Blusztajn, J., Shu, Y., Kurz, M.D., Le Roux, V., 2018. Barium isotope evidence for pervasive sediment recycling in the upper mantle. Sci. Adv. 4, eaas8675.

Niu, Y., O'Hara, M.J., 2003. Origin of ocean island basalts: a new perspective from petrology, geochemistry, and mineral physics considerations. J. Geophys. Res., Solid Earth 108.

Niu, Y., Collerson, K.D., Batiza, R., Wendt, J.I., Regelous, M., 1999. Origin of enriched-type mid-ocean ridge basalt at ridges far from mantle plumes: the East Pacific Rise at 11°20′. J. Geophys. Res., Solid Earth 104, 7067–7087.

Niu, Y., Regelous, M., Wendt, I.J., Batiza, R., O'Hara, M.J., 2002. Geochemistry of near-EPR seamounts: importance of source vs. process and the origin of enriched mantle component. Earth Planet. Sci. Lett. 199, 327–345.

Niu, Y.L., 1997. Mantle melting and melt extraction processes beneath ocean ridges: evidence from abyssal peridotites. J. Petrol. 38, 1047–1074.

Plank, T., Langmuir, C.H., 1998. The chemical composition of subducting sediment and its consequences for the crust and mantle. Chem. Geol. 145, 325–394.

Regelous, M., Niu, Y., Wendt, J., Batiza, R., Grieg, A., Collerson, K., 1999. Variations in the geochemistry of magmatism on the East Pacific Rise at 10°30′N since 800 ka. Earth Planet. Sci. Lett. 168, 45–63.

Rehkämper, M., Hofmann, A., 1997. Recycled ocean crust and sediment in Indian Ocean MORB. Earth Planet. Sci. Lett. 147, 93–106.

Rudnick, R., Gao, S., 2003. Composition of the continental crust. In: Holland, H.D., Turekian, K.K., Rudnick, R.L. (Eds.), The Crust. In: Treatise on Geochemistry, vol. 3. Elsevier-Pergamon, Oxford, pp. 1–64.

Salters, V.J.M., Stracke, A., 2004. Composition of the depleted mantle. Geochem. Geophys. Geosyst. 5, Q05B07.

Skora, S., Freymuth, H., Blundy, J., Elliott, T., Guillong, M., 2017. An experimental study of the behaviour of cerium/molybdenum ratios during subduction: implications for tracing the slab component in the Lesser Antilles and Mariana Arc. Geochim. Cosmochim. Acta 212, 133–155.

Stracke, A., 2012. Earth's heterogeneous mantle: a product of convection-driven interaction between crust and mantle. Chem. Geol. 330–331, 274–299.

Sun, P., Niu, Y., Guo, P., Duan, M., Chen, S., Gong, H., Wang, X., Xiao, Y., 2020. Large iron isotope variation in the eastern Pacific mantle as a consequence of ancient low-degree melt metasomatism. Geochim. Cosmochim. Acta 286, 269–288.

Sun, W., Bennett, V.C., Eggins, S.M., Arculus, R.J., Perfit, M.R., 2003. Rhenium systematics in submarine MORB and back-arc basin glasses: laser ablation ICP-MS results. Chem. Geol. 196, 259–281.

Thomson, A.R., Crichton, W.A., Brodholt, J.P., Wood, I.G., Siersch, N.C., Muir, J.M.R., Dobson, D.P., Hunt, S.A., 2019. Seismic velocities of CaSiO3 perovskite can explain LLSVPs in Earth's lower mantle. Nature 572, 643–647.

Villalobos-Orchard, J., Freymuth, H., O'Driscoll, B., Elliott, T., Williams, H., Casalini, M., Willbold, M., 2020. Molybdenum isotope ratios in Izu arc basalts: the control of subduction zone fluids on compositional variations in arc volcanic systems. Geochim. Cosmochim. Acta 288, 68–82.

Voegelin, A.R., Pettke, T., Greber, N.D., von Niederhäusern, B., Nägler, T.F., 2014. Magma differentiation fractionates Mo isotope ratios: evidence from the Kos Plateau Tuff (Aegean Arc). Lithos 190–191, 440–448.

Wang, X.J., Chen, L.H., Hofmann, A.W., Hanyu, T., Kawabata, H., Zhong, Y., et al., 2018. Recycled ancient ghost carbonate in the Pitcairn mantle plume. Proc. Natl. Acad. Sci. 115, 8682–8687.

Waters, C.L., Sims, K.W.W., Perfit, M.R., Blichert-Toft, J., Blusztajn, J., 2011. Perspective on the Genesis of E-MORB from Chemical and Isotopic Heterogeneity at 9–10°N East Pacific Rise. J. Petrol. 52, 565–602.

Willbold, M., Elliott, T., 2017. Molybdenum isotope variations in magmatic rocks. Chem. Geol. 449, 253–268.

Willbold, M., Hibbert, K., Lai, Y.-J., Freymuth, H., Hin, R.C., Coath, C., Vils, F., Elliott, T., 2016. High-precision mass-dependent molybdenum isotope variations in magmatic rocks determined by double-spike MC-ICP-MS. Geostand. Geoanal. Res. 40, 389–403.

Wille, M., Nebel, O., Pettke, T., Vroon, P.Z., König, S., Schoenberg, R., 2018. Molybdenum isotope variations in calc-alkaline lavas from the Banda arc, Indonesia: assessing the effect of crystal fractionation in creating isotopically heavy continental crust. Chem. Geol. 485, 1–13.

Yang, J., Siebert, C., Barling, J., Savage, P., Liang, Y.-H., Halliday, A.N., 2015. Absence of molybdenum isotope fractionation during magmatic differentiation at Hekla volcano, Iceland. Geochim. Cosmochim. Acta 162, 126–136.

Zhang, Y., Yuan, C., Sun, M., Li, J., Long, X., Jiang, Y., Huang, Z., 2020. Molybdenum and boron isotopic evidence for carbon-recycling via carbonate dissolution in subduction zones. Geochim. Cosmochim. Acta 278, 340–352.

Zindler, A., Staudigel, H., Batiza, R., 1984. Isotope and trace element geochemistry of young Pacific seamounts: implications for the scale of upper mantle heterogeneity. Earth Planet. Sci. Lett. 70, 175–195.